Human Gait Recognition with Cane Assistive Device Using Quadratic Time-Frequency Distributions

Moeness G. Amin[1], Fauzia Ahmad[1*], Yimin D. Zhang[1], and Boualem Boashash[2]

[1] Center for Advanced Communications, Villanova University, 800 E. Lancaster Ave., Villanova, PA 19085, USA
[2] Department of Electrical Engineering, College of Engineering, Qatar University, Doha, Qatar
[*] fauzia.ahmad@villanova.edu

Abstract: **In this paper, we consider the problem of human gait recognition in the presence of a walking cane using radars. Quadratic time-frequency distributions are used to provide the local signal behavior over frequency and to detail the changes in the Doppler and micro-Doppler signatures over time. New features that capture the intrinsic differences in the time-frequency signatures of the gait observed with and without the use of a cane are proposed. Results based on real data experiments conducted in a laboratory environment are provided that validate the effectiveness of the proposed features in discriminating gait with cane from normal human gait.**

1. Introduction

There is an emerging market of personal emergency response systems, which is largely driven by fall detection technologies based on cameras and wearable devices [1-4]. The attractive attributes of radar, related to its proven technology, non-obstruction, privacy preservation and safety, have brought electromagnetic (EM) waves to the forefront of indoor monitoring modalities in competition with cameras and wearable devices. One out of three elderly will fall every year which result in injuries, reduced quality of life and, unfortunately, they represent one of the leading causes of death in the elderly population. It is important, therefore, for a sensing device to detect a fall irrespective of the preceding motion whether it is sitting, standing, or walking.

Many elderly use walking assistive devices, such as canes or walkers. In this respect, falls may progress from a gait that is different from a normal arm-leg swinging motion, with the most notable difference in the case of walker assistance being in the confinement of the alternating arm swinging motion. The use of a cane, on the other hand, does not cause significant changes in the gait, aside from possible slowing of the motion speed and leg strides. This paper proposes a technique to recognize the cane assisted human gait using radar.

Radar has been shown to be an excellent sensing modality for the fall detection problem due to its capability of detecting animate targets, especially different articulations of human motions [5-10]. The general concept of radar is to transmit an EM wave over a certain range of frequencies and analyze the radar returns. It estimates the velocity of a moving object by measuring the frequency shift of the wave

radiated or scattered by the object, known as the Doppler effect. The Doppler measurement plays a fundamental role in radar systems and finds broad applications, such as the speed radars used in law enforcement and weather radars for weather forecasts [11-15]. To observe the Doppler signatures, a radar may emit narrowband continuous-wave (CW) signals, or wideband signals in the form of stepped-frequency continuous-wave signals and narrow pulse waveforms.

Radar can detect both biomechanical and biometric human signatures. The former corresponds to the gross-motor motions of different body components, such as torso, arms and legs [16-18]. The latter monitor heartbeat and respiration, which provide information about health condition and enable detection of persons in stationary activity modes [19, 20].

In this paper, we demonstrate the difference in the radar signature of the human gait observed with and without the use of a cane. Linear and quadratic time-frequency distributions, including spectrograms, are used to provide the local signal behavior over frequency and to detail the changes in the Doppler and micro-Doppler signature over time. It is shown that the motion of the cane is in sync with that of the leg motion, leading to two main changes in the gait time-frequency signal representation, namely, (a) strengthening of the radar return over one leg cycle stemming from the combined scattering from the respective leg and the cane moving in concert, (b) widening of the radar return over the same leg cycle owing to incremental time difference between the motion of the leg and that of the cane. The recognition of the cane assistive walking device helps in characterizing the proper walk, distinguishing between humans in the same range cell, and detection of the transition from a walk to a fall.

The paper is organized as follows. The signal model is presented in Section 2. Time-frequency signatures associated with human gait with and without cane are analyzed in Section 3. Section 4 proposed the features capturing the differences between the two considered gaits. Supporting results based on real data collected in a laboratory environment are provided in both Sections 3 and 4. Section 5 contains the concluding remarks.

2. Signal Model

Consider a monostatic CW radar which transmits a sinusoidal signal with frequency f_c over the sensing period. The transmitted signal is expressed as $s(t) = \exp(j2\pi f_c t)$. Consider a point target which is located at a distance of R_0 from the radar at time $t = 0$, and moves with a velocity $v(t)$ in a direction forming an angle θ with the radar line-of-sight. As such, the distance between the radar and the target at time instant *t* is given by

$$R(t) = R_0 + \int_0^t v(u)\cos(\theta)\,du. \tag{1}$$

The radar return scattered from the target can be expressed as

$$x_a(t) = \rho \exp\left[j2\pi f_c\left(t - \frac{2R(t)}{c}\right)\right], \tag{2}$$

where $\rho\ is$ the target reflection coefficient and c is the velocity of the EM wave propagation in free space. The Doppler frequency corresponding to $x_a(t)$ is given by

$$f_D(t) = 2v(t)\cos(\theta)/\lambda_c, \tag{3}$$

where $\lambda_c = c/f_c$ is the wavelength.

A spatially extended target, such as a human, can be considered as a collection of point scatterers. Therefore, the corresponding radar return is the integration over the target region and is expressed as

$$x(t) = \int_\Omega x_a(t)da. \tag{4}$$

In this case, the Doppler signature is the superposition of all component Doppler frequencies. Torso and limb motions generally generate time varying Doppler frequencies, and their exact signatures depend on the target shape and motion patterns.

3. Time-Frequency Analysis of Human Gait With and Without Cane

3.1 Time-Frequency Distributions

The radar return in (4) is nonstationary. As such, time-frequency analysis is a natural tool that reveals the time-varying Doppler and micro-Doppler frequency signatures with enhanced signal energy concentration. A number of methods are available to perform time-frequency analysis of the Doppler and micro-Doppler signatures. Time-frequency analysis methods can be generally divided into the following two classes: linear time-frequency analysis and quadratic time-frequency analysis. Short-time Fourier transform (STFT) is a commonly used technique to perform linear time-frequency analysis [21]. On the other hand, a large class of quadratic time-frequency representations is defined under the Cohen's class [22, 23].

The spectrogram $S(t, f)$, which shows how the signal power varies with time index t and frequency f, is obtained by computing the squared magnitude of STFT of the data $x(t)$ with a window $h(t)$, expressed as

$$S(t,f) = |\sum_{m=-\infty}^{\infty} h(m)x(t-m)\exp(-j2\pi fm)|^2. \quad (5)$$

On the other hand, the Cohen's class of time-frequency distribution of a signal $x(t)$ is defined as the two-dimensional Fourier transform of its kernelled ambiguity function, expressed as

$$D(t,f) = \sum_{\theta=-\infty}^{\infty}\sum_{\tau=-\infty}^{\infty} \phi(\theta,\tau)A(\theta,\tau)\exp(j4\pi f\tau - j2\pi\theta t), \quad (6)$$

where

$$A(\theta,\tau) = \sum_{u=-\infty}^{\infty} x(u+\tau)x^*(u-\tau)\exp(-j2\pi\theta u) \quad (7)$$

is the ambiguity function, $\phi(\theta,\tau)$ is the time-frequency kernel. Here, θ and τ, respectively, denote the frequency shift (also referred to as Doppler frequency) and time lag. The properties of a quadratic time-frequency distribution are heavily affected by the applied kernel.

The Wigner-Ville distribution (WVD) is often regarded as the basic or prototype quadratic time-frequency distribution, since the other Cohen's class of quadratic time-frequency distributions can be described as filtered version of the WVD. WVD is known to provide the best time-frequency resolution for single-component linear frequency modulated (LFM) signals, but it yields undesirable cross-terms when the frequency law is nonlinear or when a multi-component signal is considered. The kernel function of the WVD is unity across the entire ambiguity function.

Various reduced-interference kernels (RIDs) have been developed to reduce the cross-term interference. RID kernel $\phi(\theta,\tau)$ acts as a filter and places different weightings on the ambiguity function. Majority of signals have auto-terms located near the origin in the ambiguity domain, while the signal cross-terms are distant from the time-lag and frequency-shift axes. As such, RID kernels exhibit low-pass filter characteristics to suppress cross-terms and preserve auto-terms. For example, the Choi-Williams distribution uses a Gaussian kernel in both frequency shift and time lag axes. The kernel of the Choi-Williams distribution is expressed as $\phi(\theta,\tau) = \exp(-\mu(\theta\tau)^2)$, where μ is a constant [24].

In this paper, we use the extended modified B-distribution (EMBD) to generate the time-frequency distribution of the radar signal. It has shown that EMBD achieves better auto-term resolution and yields

improved performance for target classification [25]. The EMBS is developed based on the B-distribution kernel, which is defined as [26]

$$\phi(\theta,\tau) = g(\tau)G(\theta) = |\tau|^{\beta}\frac{|\Gamma(\beta+j\pi\theta)|^2}{2^{1-2\beta}\Gamma(2\beta)}, \tag{8}$$

for $-0.5 \le \theta \le 0.5$, $-0.5 \le \tau \le 0.5$, and $0 \le \beta \le 1$, where $\Gamma(\cdot)$ is the standard Gamma function [27]. The B-distribution kernel is the product of a low-pass filter $G(\theta)$ and a high-pass filter $g(\tau)$. The extended modified B-distribution (EMBD) is developed based on the B-distribution and exhibits improved time-frequency representation capabilities. The EMBD applies its kernel filter along both lag and Doppler axes, resulting in the expression [28]:

$$\phi(\theta,\tau) = \frac{|\Gamma(\beta+j\pi\theta)|^2}{\Gamma^2(\beta)}\frac{|\Gamma(\alpha+j\pi\tau)|^2}{\Gamma^2(\alpha)}, \tag{9}$$

where $-0.5 \le \theta \le 0.5$, $-0.5 \le \tau \le 0.5$, $0 \le \alpha \le 1$, and $0 \le \beta \le 1$. The lengths of the Doppler and lag windows are controlled by separate parameters α and β, respectively. The extra degree of freedom in the formulation of the EMBD allows to independently adjust the lengths of the windows along both lag and Doppler axes. This renders it a more useful tool for the analysis of the gait signals considered in this paper.

3.2 Experimental Setup

A CW radar was set up in the Radar Imaging Lab at Villanova University. A vertically polarized horn antenna (BAE Systems, Model H-1479) with an operational frequency range of 1–12.4 GHz and 3-dB beamwidth of 45 degrees was used as a transceiver for the CW monostatic radar. The feed point of the antenna was positioned 1.15 m above the floor. Agilent E5071B radio frequency network analyzer was used for signal generation and measurement of radar returns. A carrier frequency of 8 GHz was employed and the transmit power was set to 3 dBm. The network analyzer was externally triggered at a 1 kHz sampling rate. The record time of each experiment is 20 seconds, resulting in a total of 20,000 data samples. The radar data were collected from different human subjects with direct line of sight to the targets. Both female and male subjects were asked to walk back and forth, with and without a cane, between two points 1 and 2 located at 1 m and 4.5 m, respectively, from the antenna feed point, as shown in Fig. 1. An aluminum walking cane of length 0.94 m and diameter 2.54 cm was used and is shown in Fig. 2. The experimental studies were approved by Villanova University's Institutional Review Board and with consent from all participants.

3.3 Time-Frequency Analysis Results

We use joint time-frequency analysis methods to capture the local signal behavior over frequency and changes in Doppler and micro-Doppler signatures over time for elderly gaits with and without the use of a cane. We first compare some of the commonly used time-frequency distributions, described in Section 3.1, of the radar signal scattered from a female walking with a cane. Fig. 2a shows the spectrogram with a Hamming window of length 255, which exhibits a reasonable resolution and is free from cross-terms. The WVD, shown in Fig. 2b, depicts a high level of cross-terms because of the complicated time-frequency signatures associated with the radar return. Fig. 2c presents the Choi-Williams distribution, which provides insignificant improvement over the WVD. The corresponding EMBD result with $\alpha = 0.04$ and $\beta = 0.2$ is shown in Fig. 2d. As compared to the other distributions shown in Figs. 2a-2c, it is clear that the EMBD achieves a much clear signal representation, thereby enabling improved gait classifications. As such, we use the EMBD to perform the time-frequency analysis of the Doppler/micro-Doppler signatures in the remainder of this paper. To further demonstrate the superiority of EMBD over spectrogram in particular, we show in Section 4 that the feature extraction for human gait recognition with cane fails when employing the spectrogram based Doppler/micro-Doppler signatures.

Figure 3a depicts the time-frequency signature obtained using the EMBD with $\alpha = 0.04$ and $\beta = 0.2$ for a female walking without a cane. For convenience, the EMBD result of Fig. 2d is reproduced in Fig. 3b on a 35 dB dynamic range. In both Figs. 3a and 3b, the strongest components correspond to the main motion of the torso, whereas the relatively weaker components capture the movements of the limbs (and cane in the case of Fig. 3b). Comparing Figs. 3a and 3b, we observe the following two intrinsic differences. First, the radar return over one leg cycle is strengthened in the presence of the cane. This is because the motion of the cane is in sync with that of the leg, which causes an increase in intensity due to the combined scattering from the respective leg and the cane moving in concert. Second, owing to incremental time difference between the motion of the leg and that of the cane, the radar signature over one leg cycle is broader compared to that of the other leg cycle.

4. Time-Frequency Features for Human Gait Recognition with Cane

In this section, we identify the features that capture the differences, mentioned in Section 3.3, between the Doppler and micro-Doppler signatures of human gait with and without cane, thereby permitting discrimination between the aforementioned gaits.

4.1 Distinguishing Features

In order to effectively capture the aforementioned differences between the time-frequency signatures of the gait observed with and without the use of a cane, we consider a time slice of the EMBD corresponding to a Doppler frequency, which has been empirically determined to be 60% of the maximum Doppler frequency over the time duration of interest. The following two features extracted from the time slice are proposed:

1) *Width Ratio between Odd and Even Leg Cycles*: In order to determine the width ratio, we first obtain a binary signal $b(t)$ corresponding to each time slice by comparing the intensity at every time instant with a threshold. A unit value is assigned to $b(t)$ if the intensity exceeds the threshold; otherwise, $b(t)$ assumes a zero value. The threshold is experimentally determined to be 12.5% of the maximum intensity of the time slice. From the binary signal representation, the width ratio is defined as

$$R = \max(T_{\text{odd,avg}}/T_{\text{even,avg}}, T_{\text{even,avg}}/T_{\text{odd,avg}}), \tag{10}$$

where $T_{\text{odd,avg}}$ and $T_{\text{even,avg}}$ are the mean temporal widths of the odd and even leg cycles in the time-frequency signature. Gait signatures in the presence of a cane are expected to exhibit a width ratio much higher than unity. On the other hand, for walking without a cane, the ratio will assume values close to unity.

2) *Mean Magnitude of Intensity Difference*: The mean magnitude of intensity difference is defined as

$$\overline{\Delta} = (|\delta_1| + |\delta_2|)/2 \tag{11}$$

where δ_1 and δ_2 are the intensity differences between three consecutive peaks of the limb signatures. Since the peak intensity values exhibit relatively large variations between the left and right leg cycles in the presence of a cane, the parameter $\overline{\Delta}$ is expected to assume high values as compared to the case of the gait without the cane.

4.2 Experiment Results

The classification is performed based on the representative EMBD results of the considered human gait patterns as depicted in Fig. 3. We focus on a 7-second window of the time-frequency signature where the human subjects are moving away from the radar. As mentioned above, in order to extract the features,

namely, the width ratio and the mean magnitude of the intensity difference, we consider a time slice of the EMBD corresponding to a Doppler frequency which is 60% of the maximum Doppler frequency. In order to determine the maximum Doppler frequency over the considered 7-second window, we use a segmentation and morphological processing based technique proposed in [9] to capture the maximum Doppler frequencies at various time instances. The time slices corresponding to Figs. 4a and 4b used to extract the features are depicted in Figs. 5a and 5b, respectively.

The binary signals corresponding to the time slices in Figs. 5a and 5b are shown in Figs. 6a and 6b, respectively. The temporal support or width of each set of 'ones' in the binary signal is computed by identifying the time instants corresponding to the leftmost and the rightmost unit values. As seen from Figs. 6a and 6b, the unit values corresponding to each limb swing are not consecutive. Therefore, we define a set of 'ones' as neighboring unit values separated by no more than 0.3 seconds. The computed values of the width ratio for the time-frequency signatures of Figs. 4a and 4b are 1.67 and 4.88, respectively. For the various tested signals, the width ratio for walking with a cane varies from 2.61 to 7.89, whereas that corresponding to the signatures without the cane ranges between 1.24 and 1.67. Thus, the width ratio feature provides sufficient distinction between the two considered gaits.

For computing the mean magnitude of the intensity difference, we consider the limb swing with the maximum intensity and two neighboring limb swings, either both to its left, both to its right, or one to the left and the other to the right. The exact choice of the neighborhood is determined by the location of the second highest limb swing, whether it is consecutive to the maximum intensity swing or separated by one limb swing. The mean magnitude of the intensity difference for the time slices in Figs. 5a and 5b is equal to 0.21 and 0.68, respectively. For the various tested signals, the mean magnitude of the intensity difference for the walking with a cane is in the range [0.58, 0.87], whereas that corresponding to the signatures without a cane lies between 0.21 and 0.28. As expected, the mean magnitude of the intensity difference feature provides reasonable separability between the human gaits with and without a cane. As a result, both the width ratio and mean magnitude of intensity difference form a reasonable feature space for effective distinction between elderly walking with and without a cane.

For comparison, the time slices extracted from the spectrogram results, corresponding to the experiments considered in Figs. 4a and 4b, are depicted in Figs. 7a and 7b, respectively. The binary signals corresponding to the time slices in Figs. 7a and 7b are shown in Figs. 8a and 8b, respectively. Clearly, compared to their EMBD based counterparts, the time slices extracted from the spectrogram fail to provide a reliable feature extraction, owing to the coarse nature and higher noise floor of the spectrogram result.

4.3 Effect of Oblique Aspect Angles

In this section, we examine the impact of an oblique aspect angle on the aforementioned features that capture the differences between the time-frequency signatures of the gait observed with and without the use of a cane. We repeated the experiments described in Section 3.2 with the exception that the test subjects were asked to walk back and forth, with and without a cane, between points $1'$ and $2'$, as shown in Fig. 1. Figs. 9a and 10a depict the respective time-frequency signatures obtained using the EMBD with $\alpha = 0.04$ and $\beta = 0.2$ for a female walking between points $1'$ and $2'$ with and without a cane. Comparing Figs. 9a and 10a, we observe that the difference in widths of the radar return over the odd and even leg cycles in case of walking with a cane is somewhat preserved under oblique aspect angle. On the other hand, the strengthening of the radar return over one leg cycle in the presence of a cane no longer appears to be a prominent feature. This is because one of the legs is partially obscured from the radar in the case of oblique aspect angle, resulting in slightly different strengths of the leg returns even when the subject is not using the cane. These observations are further validated by observing Figs. 9b-9c and 10b-10c, which depict the time slices of the respective EMBD results and the corresponding binary signals. The computed values of the width ratio for the time-frequency signatures of Figs. 9a and 10a are 3.18 and 2.85, respectively, while those of the mean magnitude of the intensity difference equal 0.82 and 2.278, respectively. For the various tested signals, the width ratio for walking with a cane under oblique aspect angle varies between 2.81 and 3.18, whereas that corresponding to the signatures without the cane ranges from 1.71 to 2.85. Thus, the width ratio feature provides sufficient separability between the two considered gaits. Across the tested signals, the mean magnitude of the intensity difference for the walking with a cane takes values in the range [0.58, 0.88], whereas that corresponding to the signatures without a cane lies between 0.52 and 2.28. Thus, the mean magnitude of the intensity difference feature is unable to distinguish between the human gaits with and without a cane under an oblique aspect angle.

It is noted that motion classification under oblique incidence has always been challenging. As shown above, this problem persists for the human gait recognition with cane assistive device as well. For other human gait classification problems, efforts have previously been invested in determining what features should be selected to overcome the difficulties that arise for the case of oblique aspect angles [16, 17]. Similar investigations are warranted for the problem at hand.

5. Conclusion

We considered the problem of discriminating human gait with a walking cane from that without a cane using radars. We used time-frequency signal representations to provide the time-varying Doppler and micro-Doppler signatures corresponding to the considered gaits. Two features, namely, the width ratio and the mean magnitude of the intensity difference, were extracted, which capture the key differences in the time-frequency signatures of the gaits observed with and without the use of a cane. Real data results based on laboratory experiments were provided, which showed that the width ratio provides reliable performance under both 0° and oblique aspect angles, while the performance of the mean magnitude of the intensity difference suffers under oblique incidence.

6. Acknowledgment

This paper is made possible by NPRP Grant # NPRP 6-680-2-282 from the Qatar National Research Fund (a member of Qatar Foundation). The statements made herein are solely the responsibility of the authors.

7. References

[1] AARP, 'Health Innovation Frontiers: Untapped Market Opportunities for the 50+' (2013). Available at http://health50.org/files/2013/05/AARPHealthInnovationFullReportFINAL.pdf

[2] Noury, N. et. al: 'Fall detection - principles and methods'. Proc. Annual Int. Conf. Engineering in Medicine and Biology Society, 2007, pp. 1663–1666

[3] Perry, J. et. al: 'Survey and evaluation of real-time fall detection approaches'. Proc. Int. Symp. High-Capacity Optical Networks and Enabling Technologies, 2009, pp. 158–164

[4] Hijaz, F., Afzal, N., Ahmad, T., Hasan, O.: 'Survey of fall detection and daily activity monitoring techniques'. Proc. Int. Conf. Information and Emerging Technologies, 2010, pp. 1–6

[5] Liu, L. et. al: 'Automatic fall detection based on Doppler radar motion signature'. Proc. Int. Conf. Pervasive Computing Technologies for Healthcare and Workshops, 2011.

[6] Mercuri, M., Schreurs, D., Leroux, P.: 'SFCW microwave radar for in-door fall detection'. Proc. IEEE Topical Conf. Biomedical Wireless Technologies, Networks, and Sensing Systems, 2012, pp. 53-56

[7] Wu, M. et. al: 'Fall detection based on sequential modeling of radar signal time-frequency features'. Proc. IEEE Int. Conf. Healthcare Informatics, Philadelphia, PA, 2013.

[8] Gadde, A., Amin, M.G., Zhang, Y.D., Ahmad, F.: 'Fall detection and classifications based on time-scale radar signal characteristics'. *Proc. SPIE Radar Sensor Technology Conference*, May 2014.

[9] Wu, Q., Zhang, Y.D., Tao, W., Amin, M.G.: 'Radar-based fall detection based on Doppler time-frequency signatures for assisted living', *IET Radar, Sonar & Navigation*, **9**, (2), 2015, pp. 164-172

[10] Jokanovic, B., Amin, M.G., Zhang, Y.D., Ahmad, F.: 'Multi-window time-frequency signature reconstruction from undersampled continuous wave radar measurements for fall detection', *IET Radar, Sonar & Navigation*, **9**, (2), 2015, pp. 173-183

[11] Chen, V. C., Ling, H.: 'Time-Frequency Transforms for Radar Imaging and Signal Analysis' (Artech House, 2002)

[12] Doviak, R.J., Zrnic, D.S.: 'Doppler Radar and Weather Observations' (Second Edition. Dover, 2006)

[13] Chen, V.C.: 'The Micro-Doppler Effect in Radar' (Artech House, 2011)

[14] Chen, V. C., Tahmoush, D., Miceli, W. J.: 'Radar Micro-Doppler Signature: Processing and Applications' (IET digital library, 2014)

[15] Stanković, L.J., Daković, M., Thayaparan, T.: 'Time-Frequency Signal Analysis with Applications' (Artech House, 2013)

[16] Mobasseri, B., Amin, M.G.: 'A time-frequency classifier for human gait recognition'. Proc. SPIE Conf. Optics and Photonics in Global Homeland Security V and Biometric Technology for Human Identification VI , **7306**, 2009

[17] Tivive, F.C., Bouzerdoum, A., Amin, M.G.:'A human gait classification method based on radar Doppler spectrograms', EURASIP Journal on Advances in Signal Processing, **2010**, Article ID 389716, 2010

[18] Orović, I., Stanković, S., Amin, M.: 'A new approach for classification of human gait based on time-frequency feature representations', Signal Processing, **91**, (6), 2011, pp. 1448–1456

[19] Høst-Madsen, A. et. al: 'Signal processing methods for Doppler radar heart rate monitoring', in D. Mandic, M. Golz, A. Kuh, D. Obradovic, and T. Tanaka (Eds.), Signal Processing Techniques for Knowledge Extraction and Information Fusion (Springer, 2008), pp. 121-140

[20] Aardal, O., Hamran, S-E., Berger, T., Hammerstad, J., Lande, T.S.; 'Radar cross section of the human heartbeat and respiration in the 500MHz to 3GHz band'. Proc. IEEE Radio and Wireless Symp., 2011, pp. 422–425

[21] Almeida, L. B.: 'The fractional Fourier transform and time-frequency representations', IEEE Trans. Signal Proc., 1994, **42**, (11), pp. 3084–3091

[22] Cohen, L.: 'Time-frequency distributions - a review', Proc. IEEE, 1989, **77**, (7), pp. 941–981

[23] Cohen, L.: 'Time-Frequency Analysis' (Englewood Cliffs, NJ: Prentice Hall, 1995)

[24] Choi, H., Williams, W. J.: 'Improved time-frequency representation of multicomponent signals using exponential kernels,' IEEE. Trans. Acoustics, Speech, Signal Processing, 1989, **37**, (6), pp. 862–871

[25] Boashash, B., Khana, N. A., and Ben-Jabeura, T.: 'Time–frequency features for pattern recognition using high-resolution TFDs: A tutorial review, ' Digital Signal Processing, in press. Available at http://www.sciencedirect.com/science/article/pii/S1051200414003571

[26] Boashash, B.: 'Time-Frequency Signal Analysis and Processing: A Comprehensive Reference' (Elsevier, Oxford, 2003)

[27] Abramowitz, M., Stegun, I.: 'Handbook of Mathematical Functions' (New York: Dover, 1972)

[28] Boashash, B., Ben-Jabeur, T.: 'Design of a high-resolution separable-kernel quadratic TFD for improving newborn health outcomes using fetal movement detection'. Proc. Int. Conf. Information Science, Signal Proc. and Their Applications, Montreal, Canada, 2012, pp. 354–359

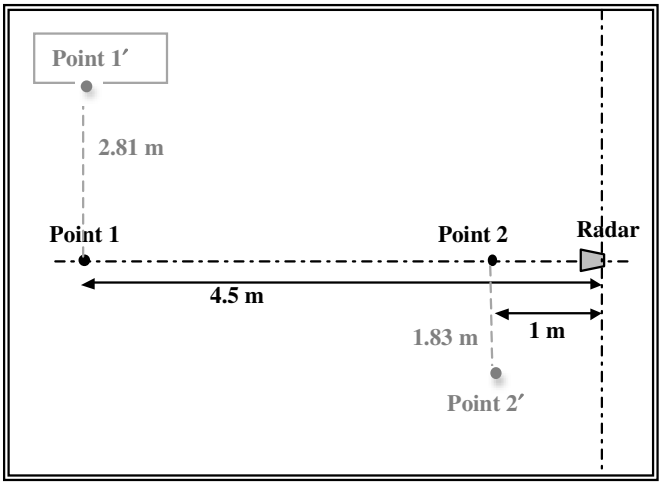

Fig. 1. *Scene Layout.*

Fig. 2. *Aluminum cane.*

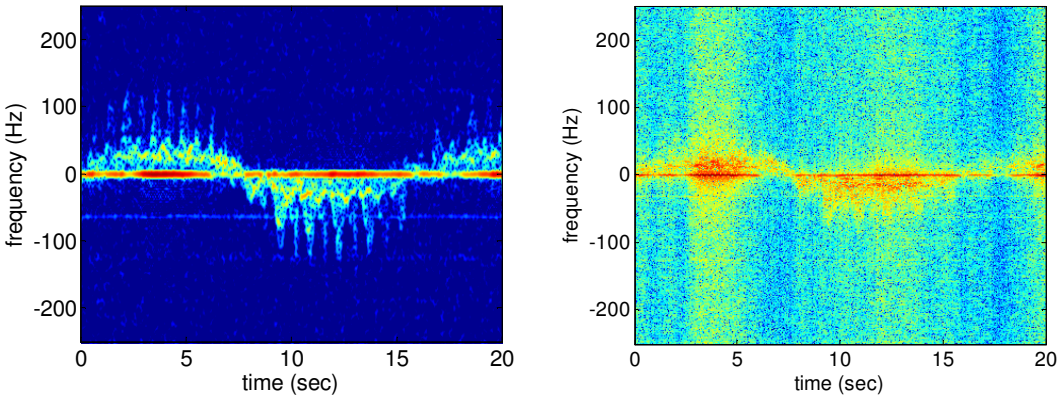

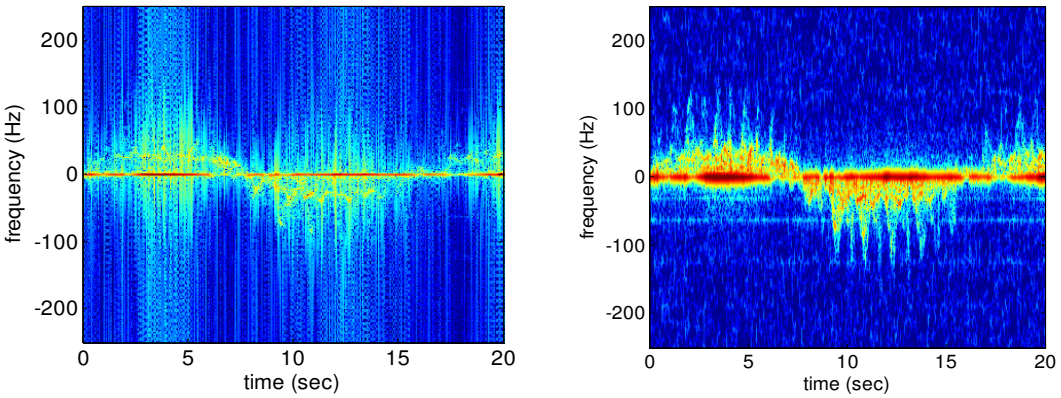

Fig. 3. *Different time-frequency distributions of a radar return from a female walking with a cane*
a Spectrogram
b Wigner-Ville distribution
c Choi-Williams distribution
d Extended modified B-distribution

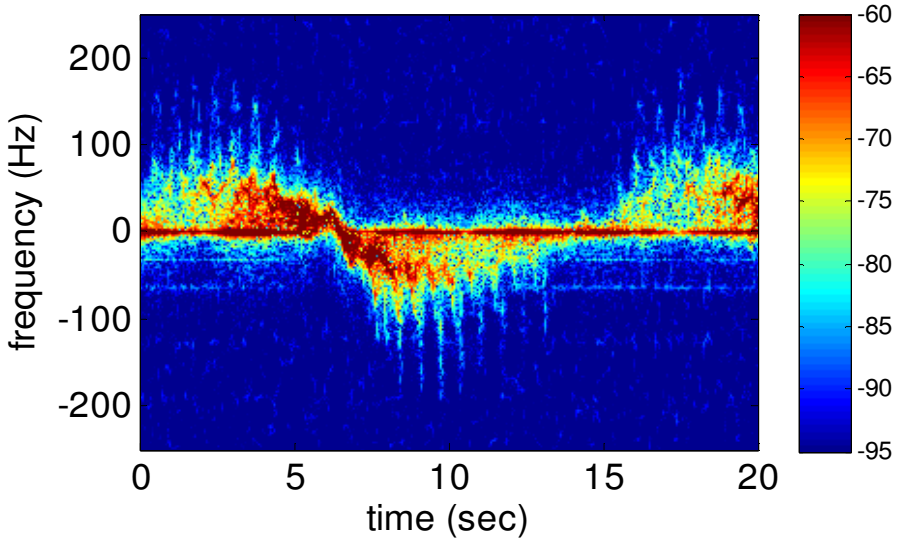

a

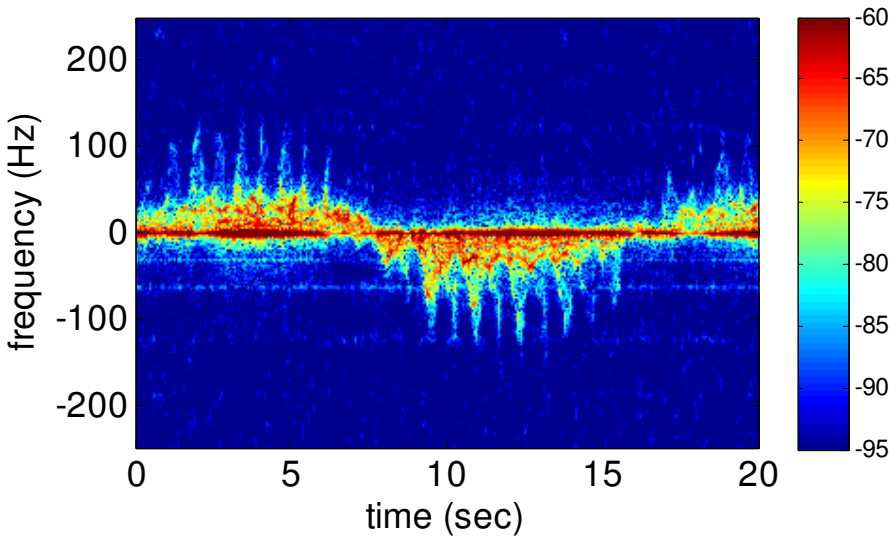

b

Fig. 4. *EMBD results of a radar return from a female*
a Walking without a cane
b Walking with a cane

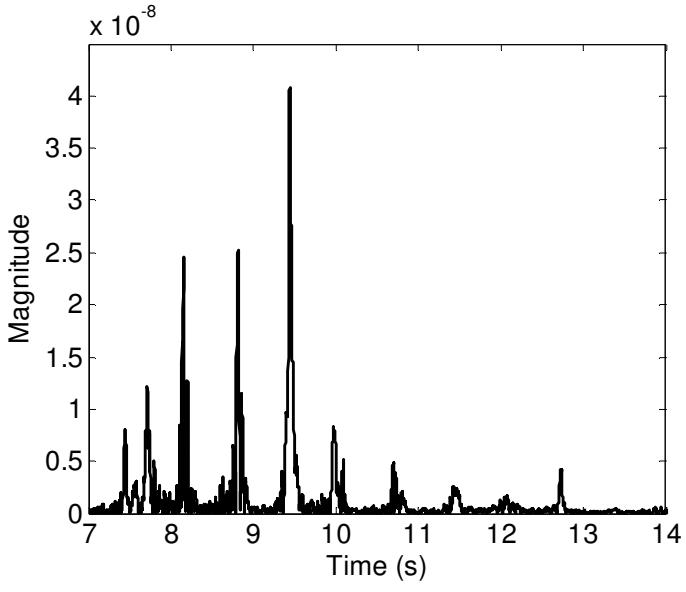

a

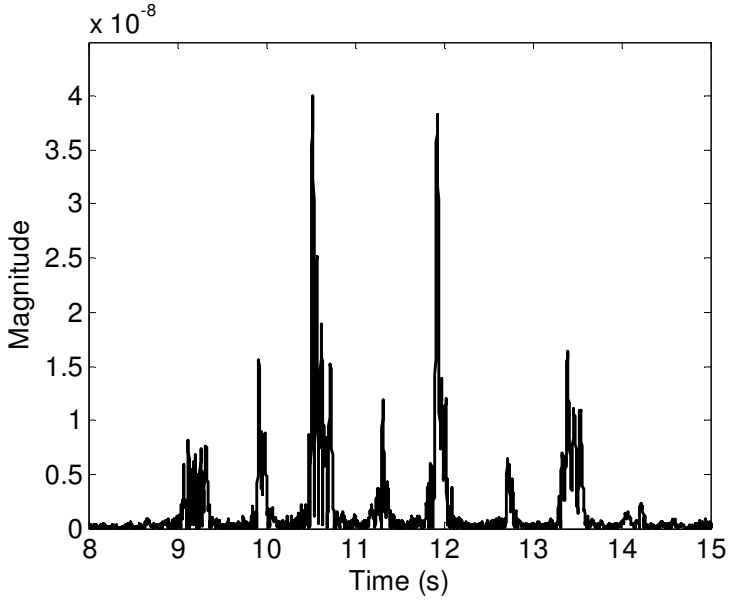

b

Fig. 5. *Time slices extracted from the EMBD results of Fig. 4.*
a Walking without a cane
b Walking with a cane

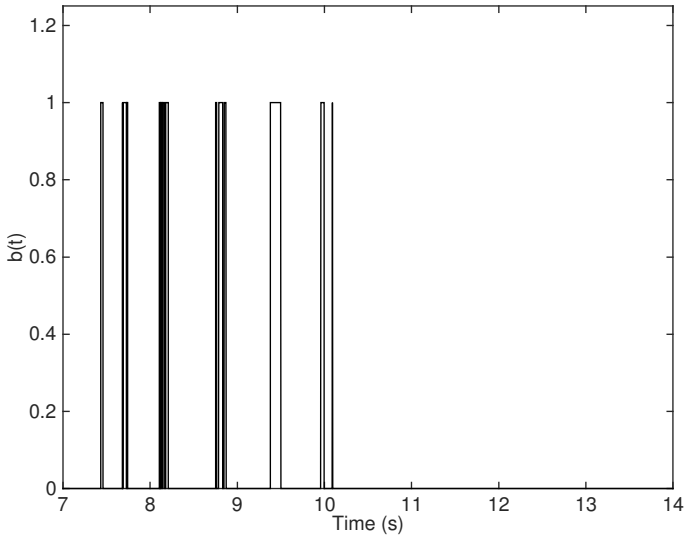

a

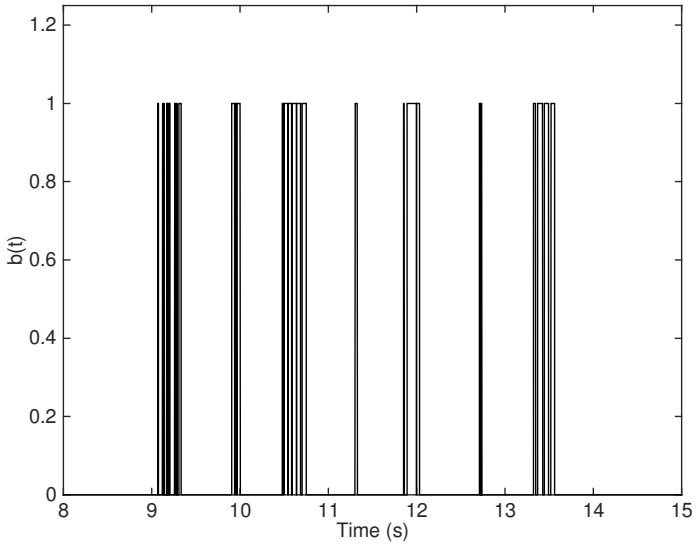

b

Fig. 6. *Binary signals corresponding to time slices of Fig. 5.*
a Walking without a cane
b Walking with a cane

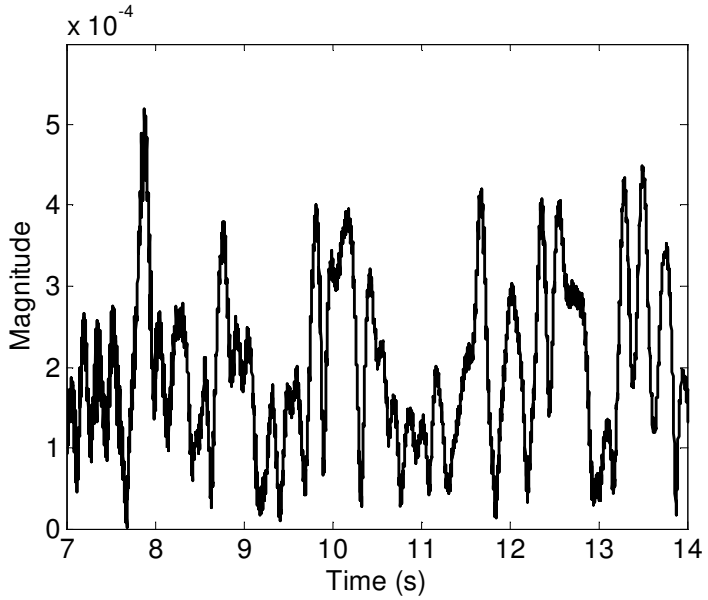

a

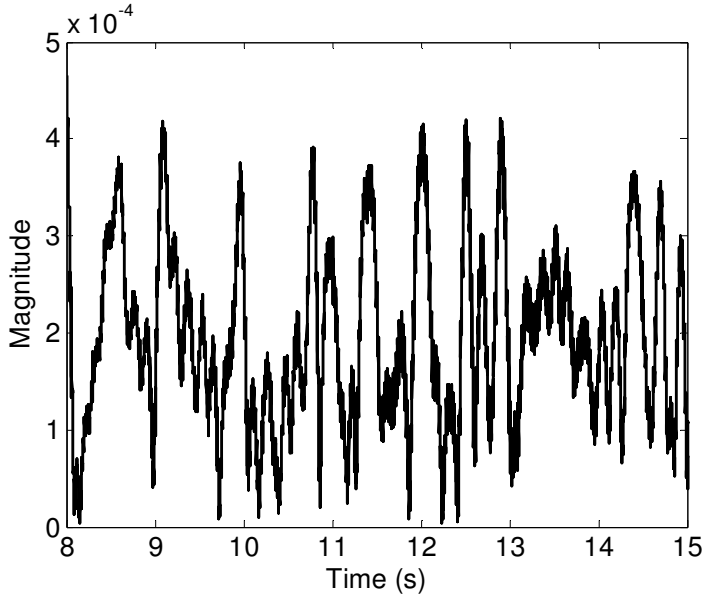

b

Fig. 7. *Time slices extracted from the Spectrogram results of a radar return from a female* (*same experiment as in Fig. 3*)
a Walking without a cane
b Walking with a cane

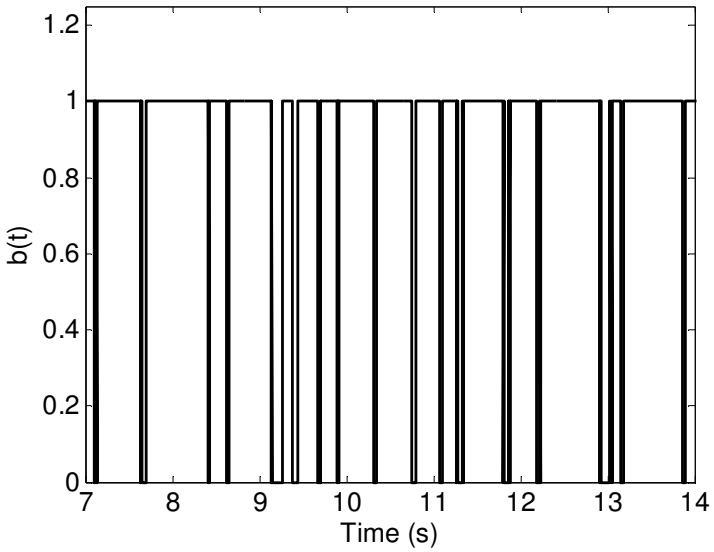

a

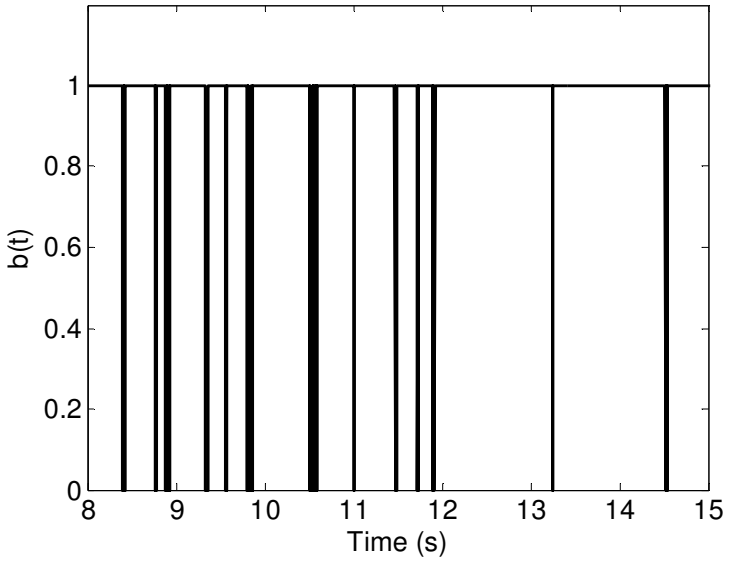

b

Fig. 8. *Binary signals corresponding to time slices of Fig. 7.*
a Walking without a cane
b Walking with a cane

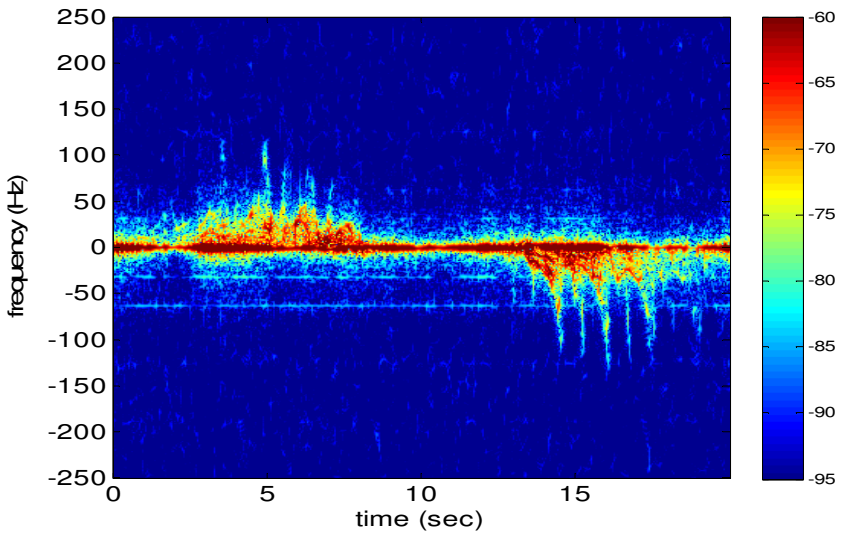

a

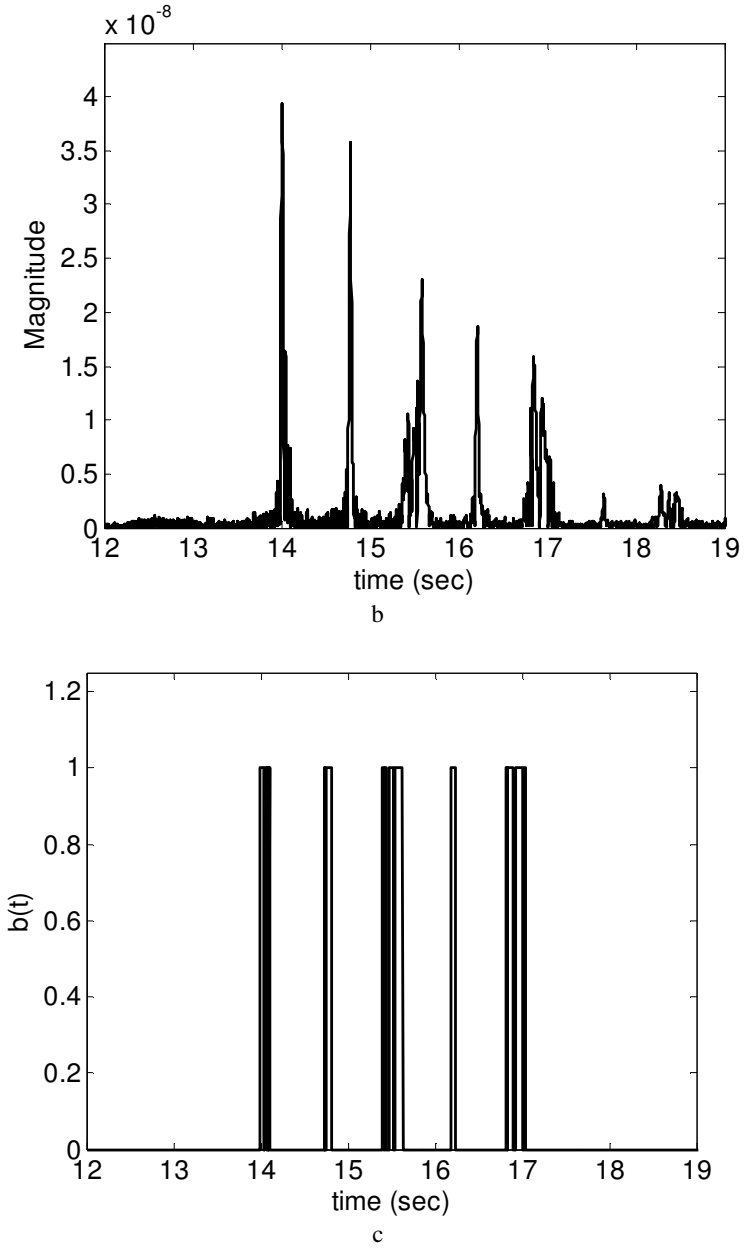

Fig. 9. *Time-frequency representation of a radar return at an oblique aspect angle from a female walking with a cane.*
a EMBD result
b Time slice
c Binary signal

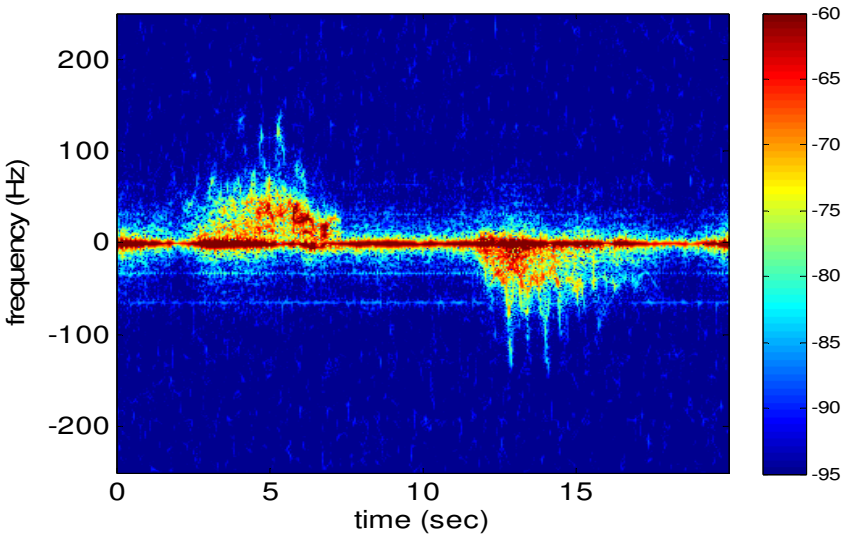
frequency (Hz)
200
100
0
-100
-200
0
5
10
15
time (sec)
-60
-65
-70
-75
-80
-85
-90
-95

a

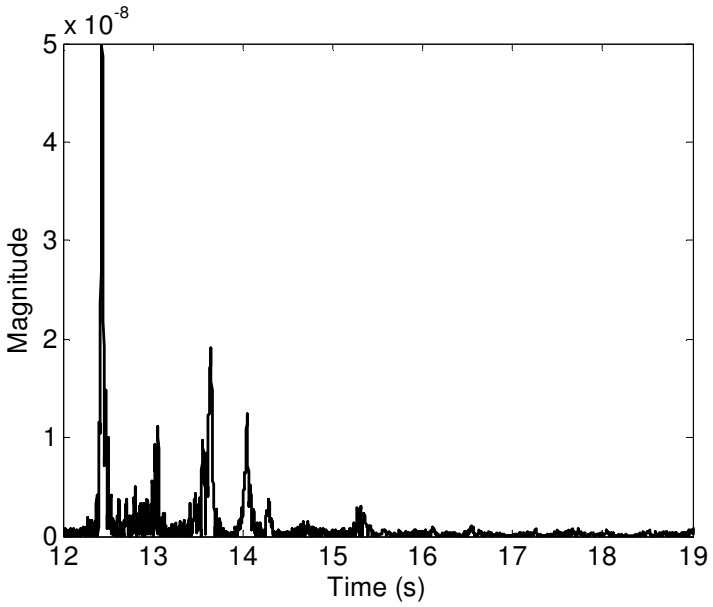
x 10^-8
Magnitude
5
4
3
2
1
0
12
13
14
15
16
17
18
19
Time (s)

b

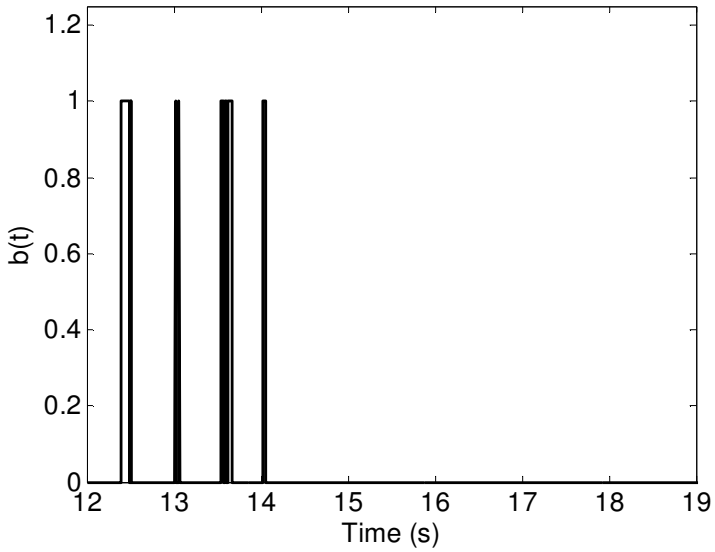

c

Fig. 10. *Time-frequency representation of a radar return at an oblique aspect angle from a female walking without a cane.*
a EMBD result
b Time slice
c Binary signal